ADVANCED MATERIALS

Supporting Information

for *Adv. Mater.,* DOI: 10.1002/adma.202102451

Tunable Structural Color Images by UV-Patterned Conducting Polymer Nanofilms on Metal Surfaces

*Shangzhi Chen, Stefano Rossi, Ravi Shanker, Giancarlo Cincotti, Sampath Gamage, Philipp Kühne, Vallery Stanishev, Isak Engquist, Magnus Berggren, Jesper Edberg, Vanya Darakchieva, and Magnus P. Jonsson**

Supplementary Information for

Tunable Structural Color Images by UV-Patterned Conducting Polymer Nanofilms on Metal Surfaces

Shangzhi Chen[1], Stefano Rossi[1], Ravi Shanker[1], Giancarlo Cincotti[1], Sampath Gamage[1], Philipp Kühne,[2,3], Vallery Stanishev[2], Isak Engquist[1], Magnus Berggren[1], Jesper Edberg[4], Vanya Darakchieva[2,3] and Magnus P. Jonsson[1]*

[1] Laboratory of Organic Electronics, Department of Science and Technology (ITN), Linköping University, SE-601 74 Norrköping, Sweden

[2] Terahertz Materials Analysis Center (THeMAC), Department of Physics, Chemistry and Biology (IFM), Linköping University, SE-581 83 Linköping, Sweden

[3] Center for III-Nitride Technology, C3NiT-Janzèn, Department of Physics, Chemistry and Biology (IFM), Linköping University, SE-581 83 Linköping, Sweden

[4] RISE Research Institutes of Sweden, Bio- and Organic Electronics, Bredgatan 35, SE-602 21 Norrköping, Sweden

* Correspondence: magnus.jonsson@liu.se

Part I: Supplementary Notes

Supplementary Note A

We observed an increase in surface roughness (from 13 nm to 47 nm) with increasing UV exposure time (**Figure S20**), although normal incidence reflectance spectra show a rather small percentage of non-specular scattered light (see **Figure S21**). The somewhat rough 10 min UV-patterned PEDOT films contained both small dots in sizes of tens of nanometers and concave or convex surface in sizes of 5-10 µm, which started to emerge at 3 min UV exposure as observed by optical microscopy (**Figure S22**)[1,2]. Similar features have been reported by Murphy *et al.*[3] and considered as a result of humidity-induced crystallization of iron salts ($Fe(Tos)_3$) in the oxidant film. Crystallization of iron salts weakens the coordination effect between iron ions and the tri-block co-polymer additives (see **Experimental Section**) and therefore creates more nucleation sites for film growth, largely modulating the polymerization kinetics[4]. In our case, the UV exposure step was carried out at atmospheric conditions without any special inert gas protection and samples could be affected by the humidity, especially for samples with long UV exposure times. Optical microscopy reveals two different regions: areas showing the macroscopically observed colors and small areas with dark colors that sometimes generate additional reflectance peaks or widens the reflectance peak width corresponding reduction in color purity (**Figure S23**).

To avoid this crystallization effect, we thermally annealed samples after UV patterning but prior to VPP, which largely supressed the formation of iron salt crystallites (see 'baked oxidant' in **Figure S22** and **S23**). However, the devices made using this strategy showed more limited color tuneability (**Figure S24**), where the reflectance peak only shifted between 450 nm (blue) and 570 nm (yellow-green). Further characterization of these films reveals that the thermal annealing step largely diminished the patterning effect by reducing the thickness variations and partly also the variations in the optical extinction (**Figure S25**). Ellipsometry data (**Figure S26** and **27**) show lower variations in both real and imaginary refractive index upon UV exposure of the baked oxidants, further corroborating the findings.

Therefore, there is currently a trade-off between color purity (reflectance peak width) and color gamut, which may be further optimized *via* processing parameters, such as oxidant recipes, polymerization conditions (*e.g.,* substrate temperature), and precise local environment humidity control. Although film thickness may further increase with longer UV exposure times, we restricted the time to maximum 10 min in this study, partly to avoid too rough surfaces.

Part II: Supplementary Figures

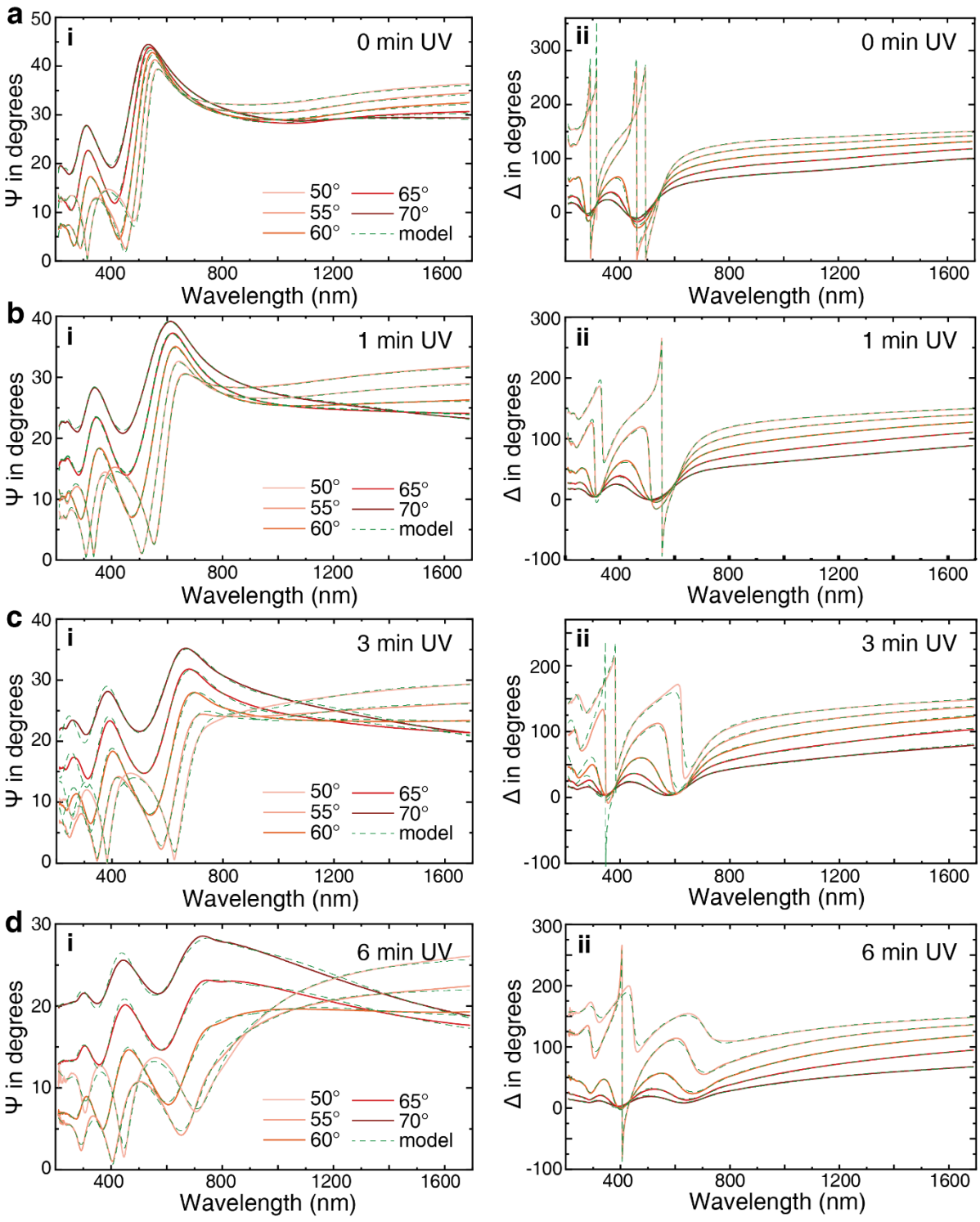

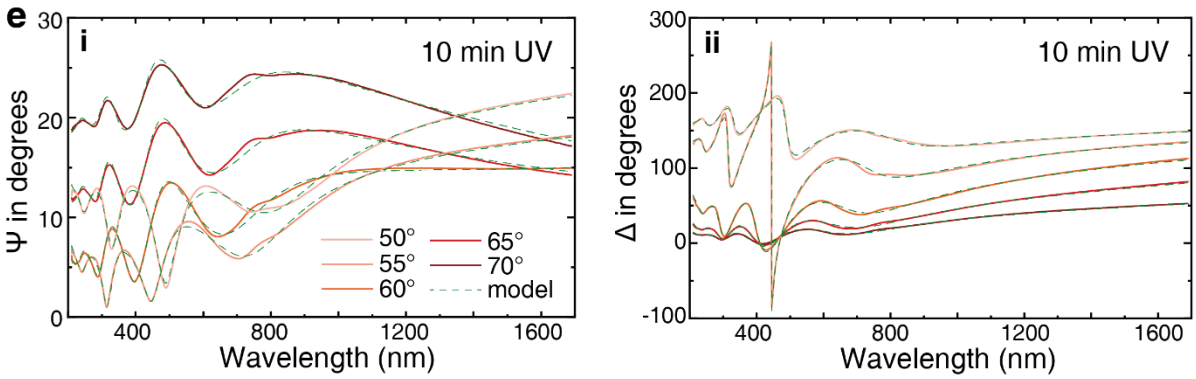

Figure S1 | Spectroscopic ellipsometry spectra for UV-treated PEDOT thin films. Five UV exposure times were used: 0 min (**a**), 1 min (**b**), 3 min (**c**), 6 min (**d**), and 10 min (**e**). For each measurement, five incident angles were used: 50°, 55°, 60°, 65°, and 70°. The Drude-Lorentz model[5] was used to fit for the data. The experimental measured data (**i** for ψ and **ii** for Δ) and model fits were plotted in red solid and green dashed curves, respectively. The UV-treated PEDOT films were deposited on sapphire substrates. The complex refractive index dispersions derived from the Drude-Lorentz model are shown in **Figure 1c, 1d,** and **S2**.

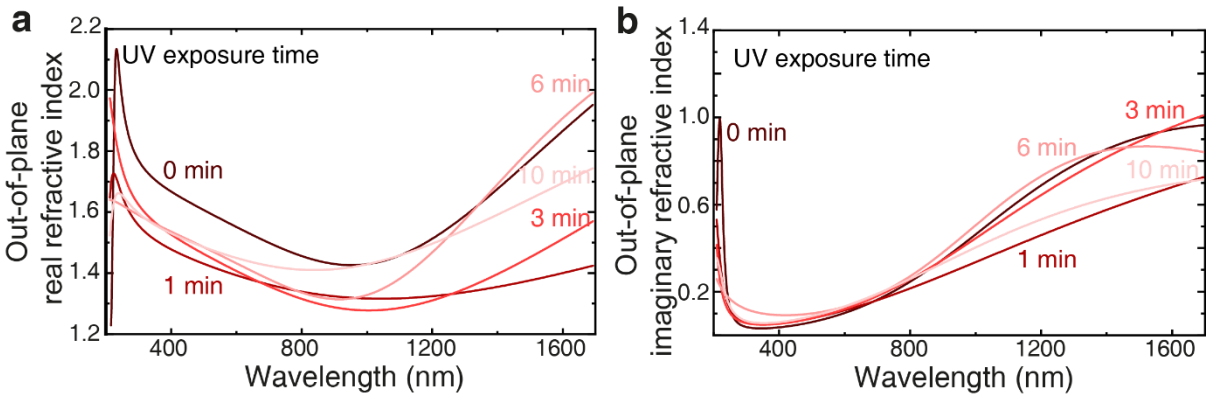

Figure S2 | Out-of-plane refractive index of UV-treated PEDOT thin films. a, Real refractive index. **b**, Imaginary refractive index. Their in-plane counterparts are shown in **Figure 1c** and **1d**. UV exposure time used were 0, 1, 3, 6, and 10 min.

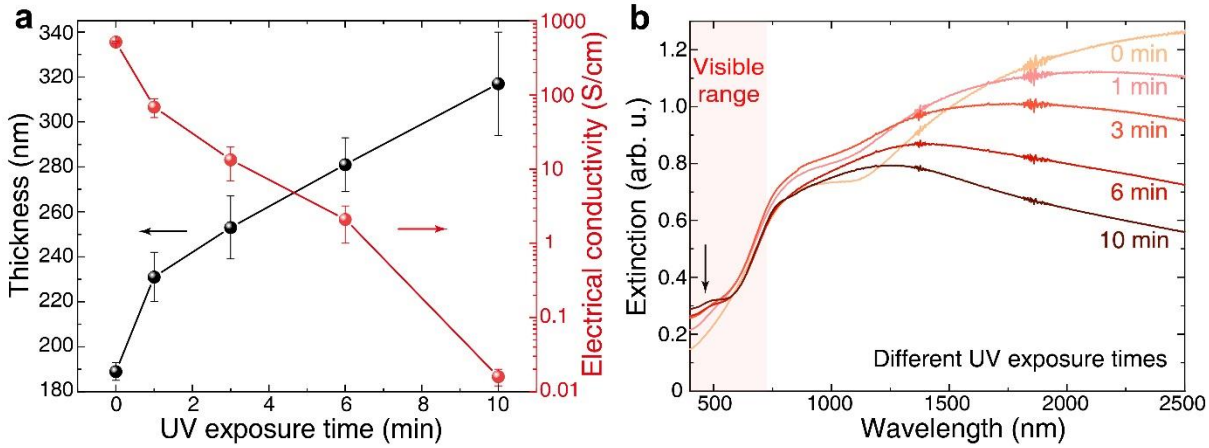

Figure S3 | Properties of UV-treated PEDOT thin films. a, Thin film thickness and electrical conductivity. **b**, Extinction spectra of PEDOT thin films prepared by exposure time ranging from 0 to 10 min and polymerization time of 60 min. The samples were prepared using microscope glass slides as substrates and the finally obtained thickness values can vary depending on the type of substrates. The light red shaded area in **b** represents the visible range. The arrow in **b** indicates the additional extinction shoulder due to the existence of short-chain polymers[1,2]. With the increase of UV exposure time, the extinction in the near infrared region decreases and short-chain polymer signal intensity at short wavelengths increases.

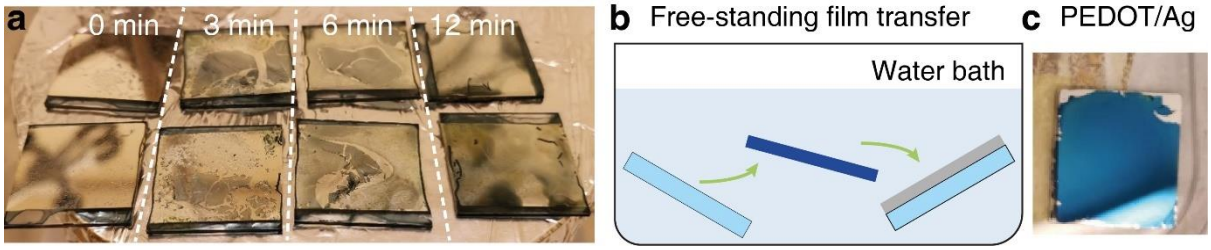

Figure S4 | Devices using silver bottom mirrors. a, UV-treated PEDOT films deposited on Ag bottom mirrors. Four different UV exposure intervals were used: 0, 3, 6, and 12 min. It was found that the oxidant can react with the Ag bottom mirror upon its deposition and no uniform films could be polymerized for these samples. In addition, Ag film is hydrophobic and no oxygen-plasma treatment should be used to improve hydrophilicity due to the potential oxidation of the Ag layer. **b**, Free-standing film transfer strategy was used to re-deposit as-formed PEDOT films to new substrates (see details in **Methods** section)[6]. PEDOT films could be delaminated in a water bath and transferred onto the Ag-coated substrates, thus avoiding direct contact between the oxidant and the Ag film. PEDOT film on a Ag-coated substrate is shown in **c**. However, for UV-treated PEDOT samples, the films showed strong adhesion to the original substrates and could hardly be transferred to the new Ag-coated substrates. Therefore, this method currently cannot be used for preparing UV-treated PEDOT on Ag bottom mirrors.

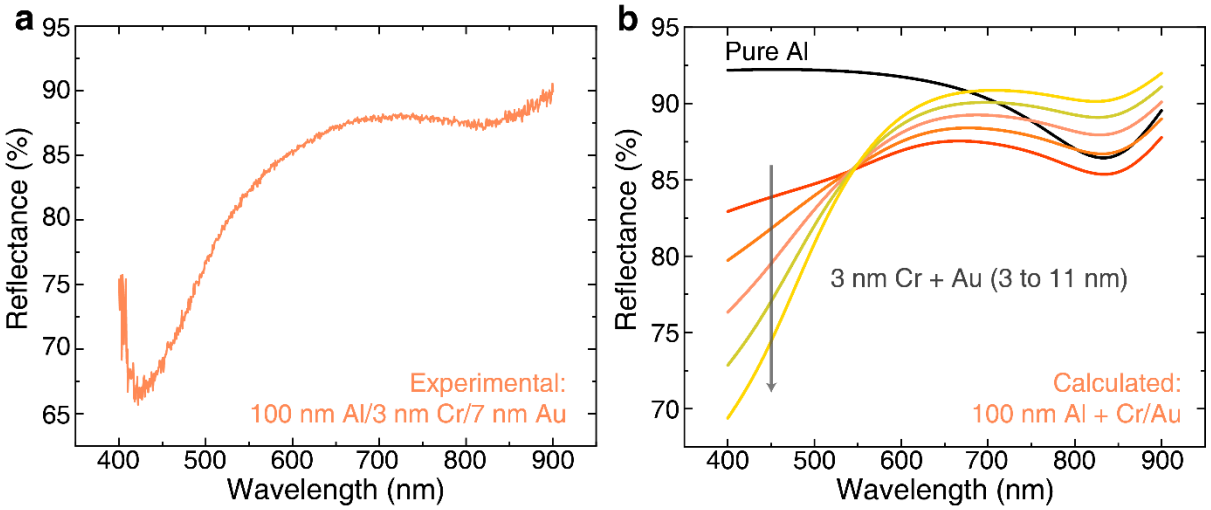

Figure S5 | Reflectance spectra of different metallic mirrors. a, Experimental reflectance curves of 7 nm Au/3 nm Cr/100 nm Al mirror. The mirror was deposited on a glass substrate. **b**, Simulated reflectance curves of 100 nm Al with different thickness combinations of Cr and Au layers. The thickness of Au is ranging from 3 nm to 11 nm in steps of 2 nm as indicated by the grey arrow. The reflectance for pure Al is included as the black line. The overall shape of the curves from the calculations matches well with the experimental curve. The difference between experiment and calculation may be due to surface roughness and poor coverage of the thin Cr and Au layer. Also, the optical parameters of ultrathin metal layer might deviate from that of the bulk.

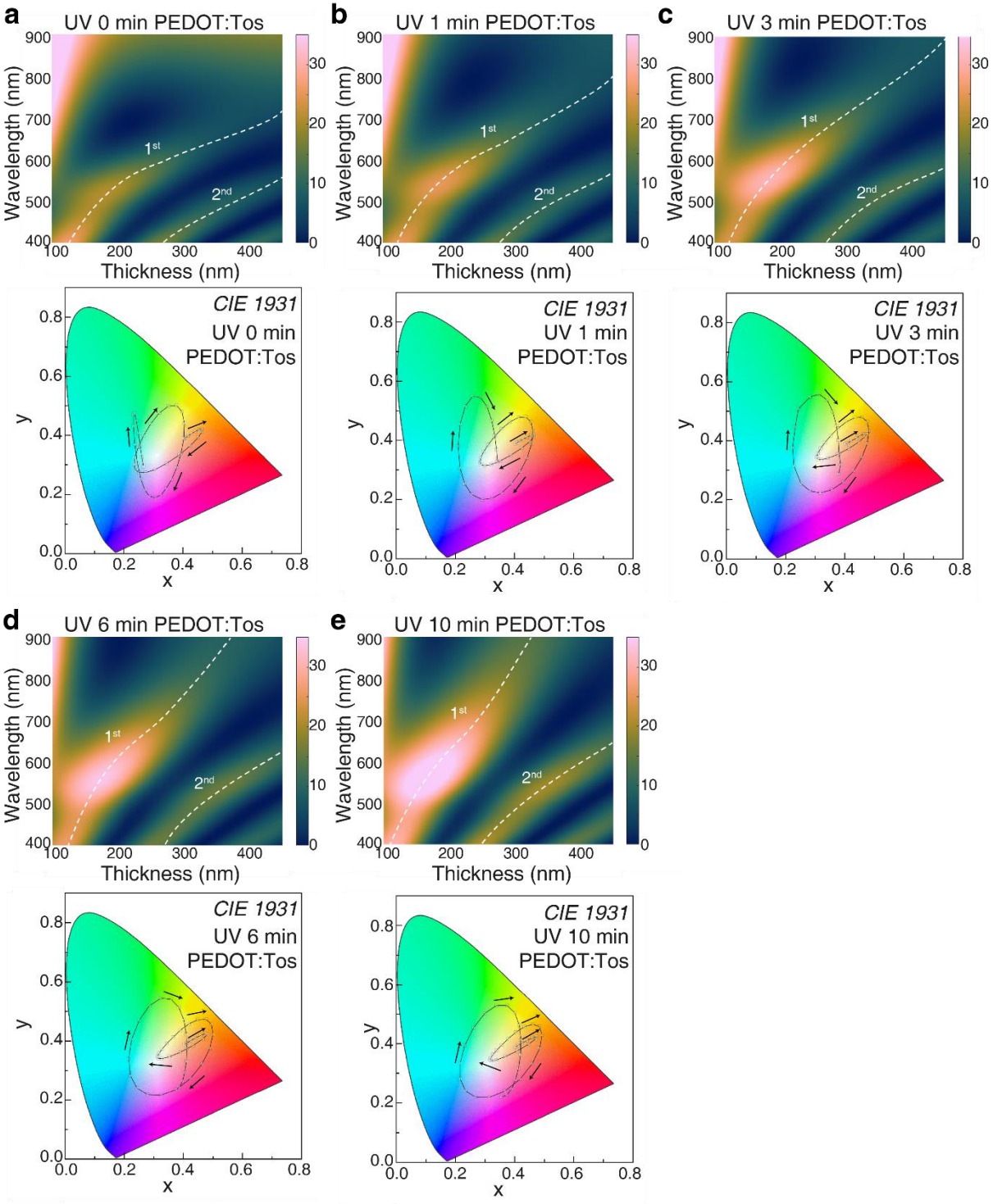

Figure S6| Simulated reflectance of UV-treated PEDOT:Tos on 100 nm Au bottom mirror. PEDOT:Tos thin films with different UV exposure times were used: 0 min (**a**), 1 min (**b**), 3 min (**c**), 6 min (**d**), and 10 min (**e**). The top panels are 2D heat maps of simulated reflectance with respect to film thickness and the bottom panels are the distribution of CIE coordinates for these devices in *CIE 1931 xy* chromaticity diagram.

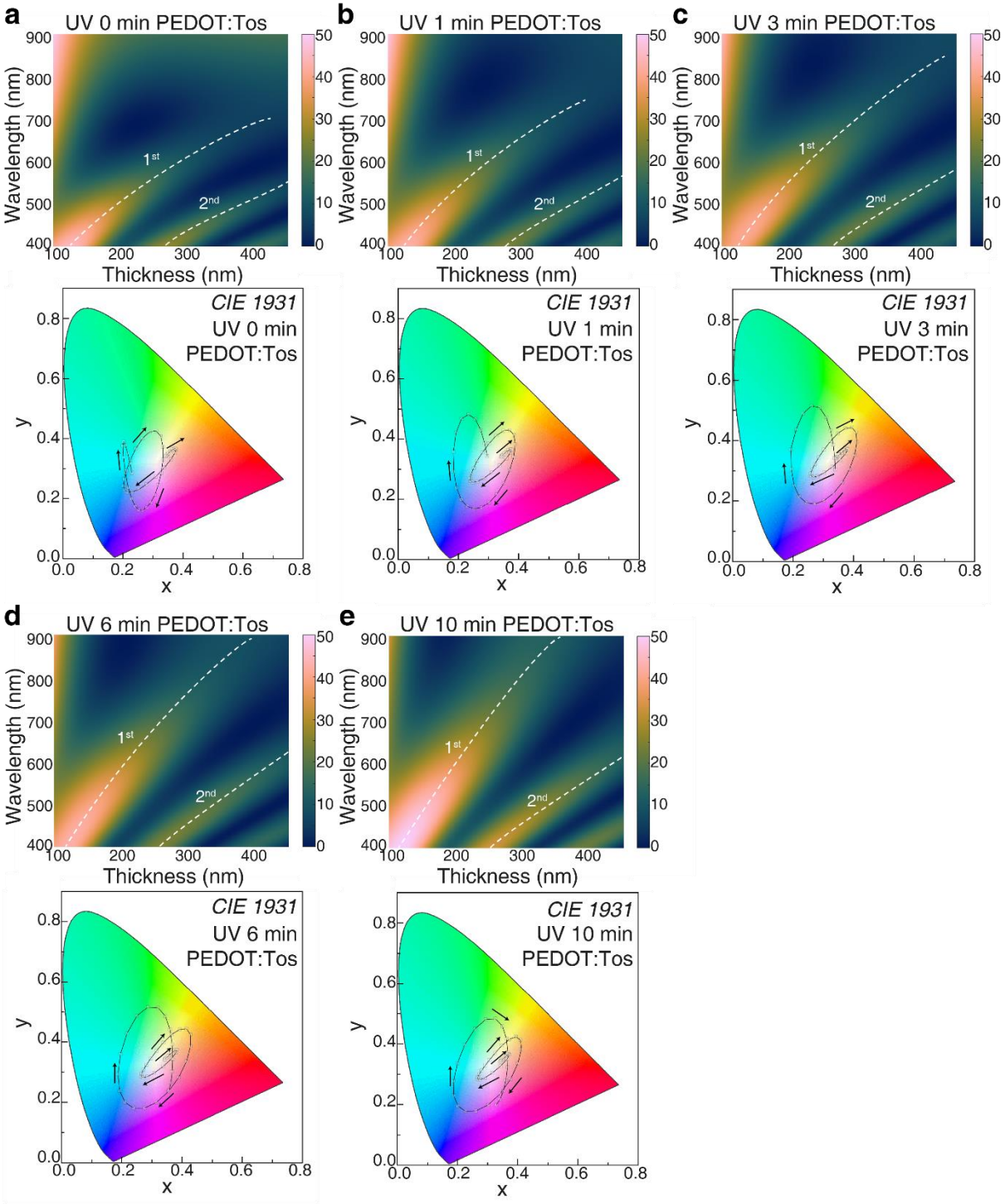

Figure S7| Simulated reflectance of UV-treated PEDOT:Tos on 7 nm Au/3 nm Cr/100 nm Al bottom mirror. PEDOT:Tos thin films with different UV exposure times: 0 min (**a**), 1 min (**b**), 3 min (**c**), 6 min (**d**), and 10 min (**e**). The top panels are 2D heat maps of simulated reflectance with respect to film thickness and the bottom panels show the distribution of CIE coordinates for these devices in *CIE 1931 xy* chromaticity diagram.

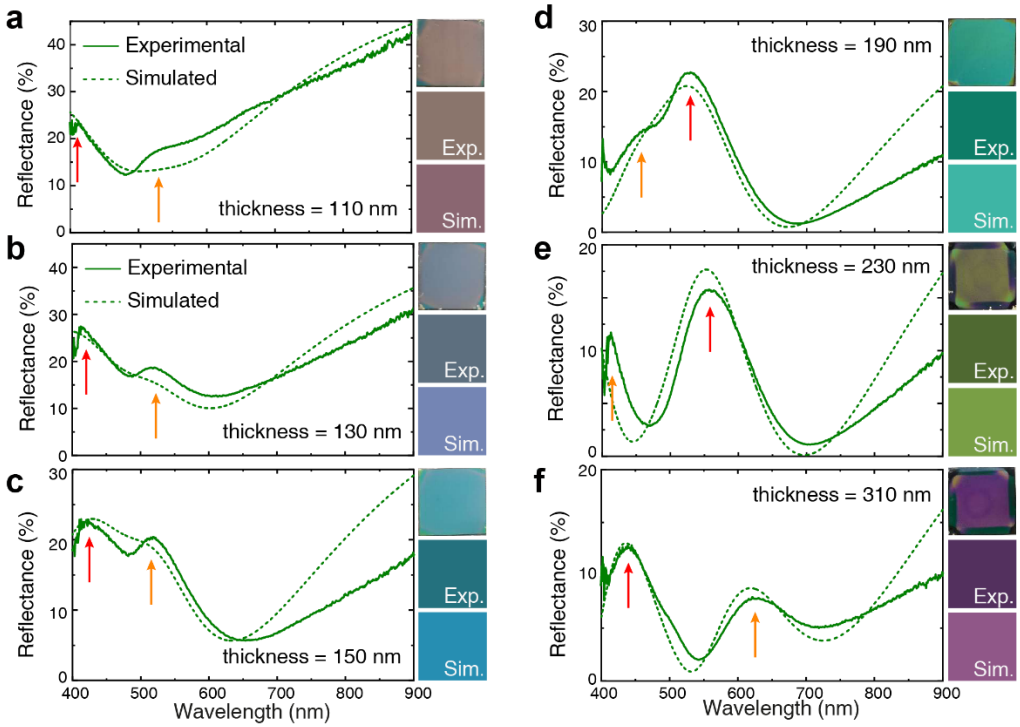

Figure S8 | Structural colors of PEDOT by only tuning film thicknesses. PEDOT:Tos with no UV treatments were prepared with different thicknesses: 110 nm (a), 130 nm (b), 150 nm (c), 190 nm (d), 230 nm (e), and 310 nm (f). 100 nm bottom Au mirrors were used. Experimental (solid) and simulated (dashed) reflectance spectra are presented. The panels to the right of each graph display sample photographs (1st row) and pseudocolors obtained from CIE coordinates based on experimental (2nd row) and simulated reflectance curves (3rd row). The generated reflective colors from pink-grey (thickness of 110 nm) to yellow-green (thickness of 230 nm), with corresponding primary reflectance peak positions varying from 410 nm to 570 nm, agreeing well with simulated results. A 2nd order reflectance peak becomes dominant for larger thicknesses of about 250 nm (with the 1st order peak located at around 590 nm), which limits pure color generation at longer wavelengths (*e.g.* yellow and red).

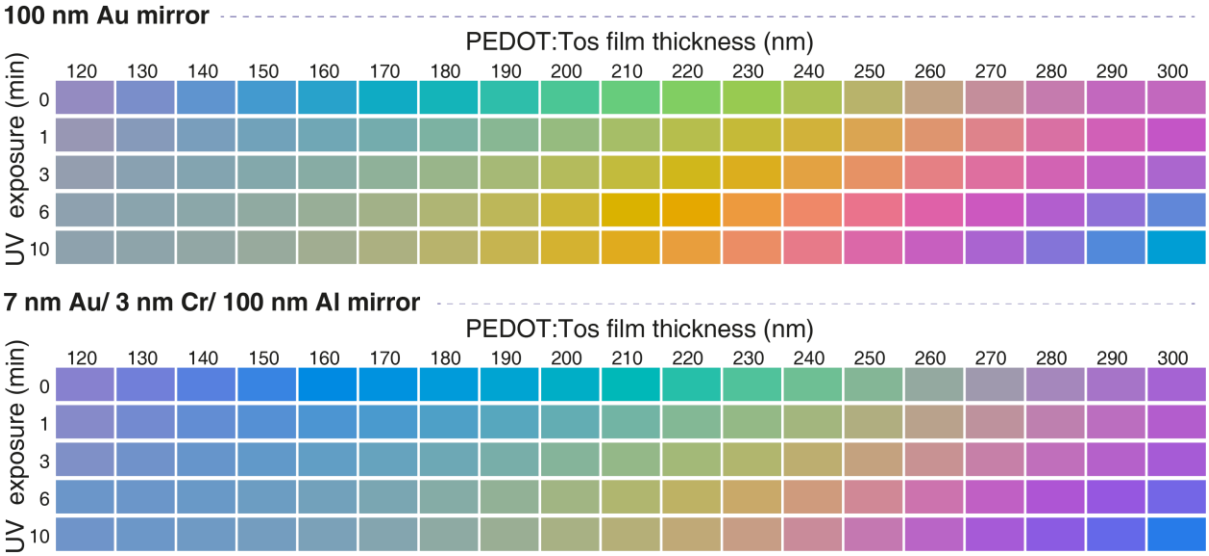

Figure S9 | Pseudocolors based on simulated reflectance spectra. CIE coordinates were obtained from simulated reflectance spectra (**Figure S6 and S7**) to create pseudocolors. The top panel is for 100 nm Au bottom mirror while the bottom panel is for 7 nm Au/3 nm Cr/100 nm Al bottom mirror. The *x*-axis is the thickness of the PEDOT:Tos film and the *y*-axis is the UV exposure time. It is clear that UV exposure (modulating both film thickness and absorption profiles) can widen the color ranges by creating more longer wavelength colors (*e.g.* yellow and red) than only tuning thickness.

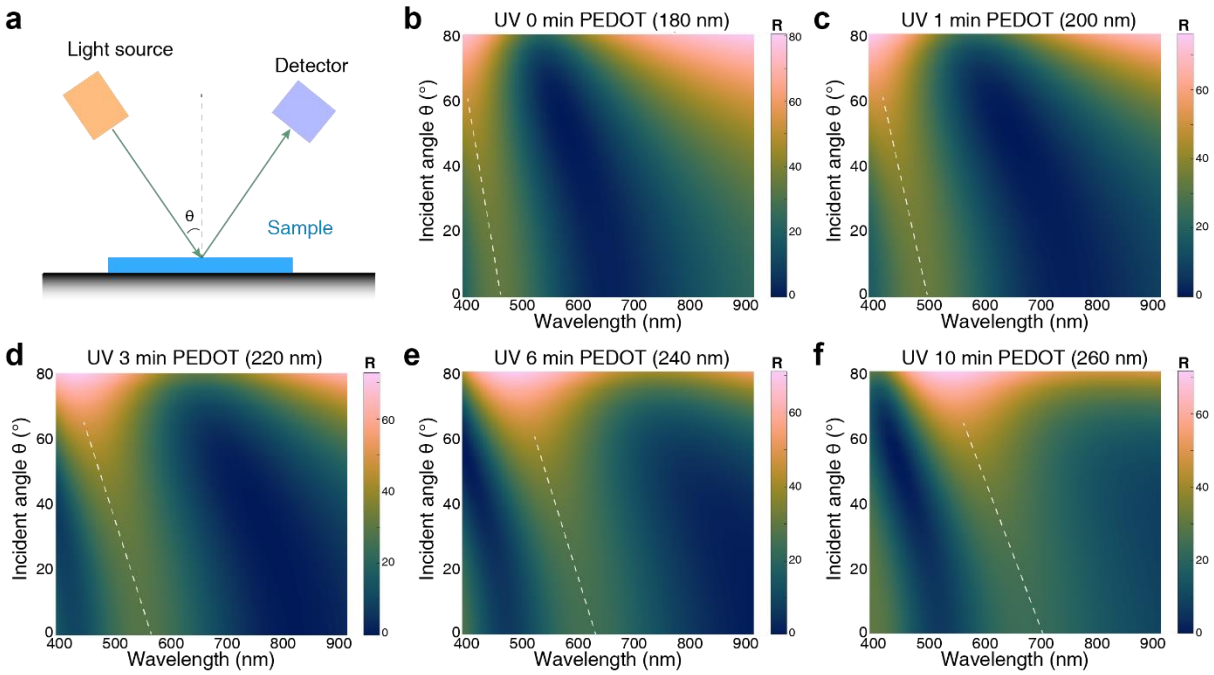

Figure S10 | Incident angle dependence of calculated reflectance. a, Illustration of setup analogues to that used for the calculations, where the incident angle θ is defined as the angle between incident (outgoing) ray and surface normal. **b-e**, 2D heat maps of reflectance spectra of UV 0 min (**b**), 1 min (**c**), 3 min (**d**), 6 min (**e**), and 10 min (**f**) PEDOT:Tos with respect to the incident angle. It can be observed that the slopes of the primary reflectance peak slightly tilt with the increase of incident angle. The reflectance curves were calculated by *stackrt* function of Lumerical FDTD solutions for s-polarization light (parallel to sample surface).

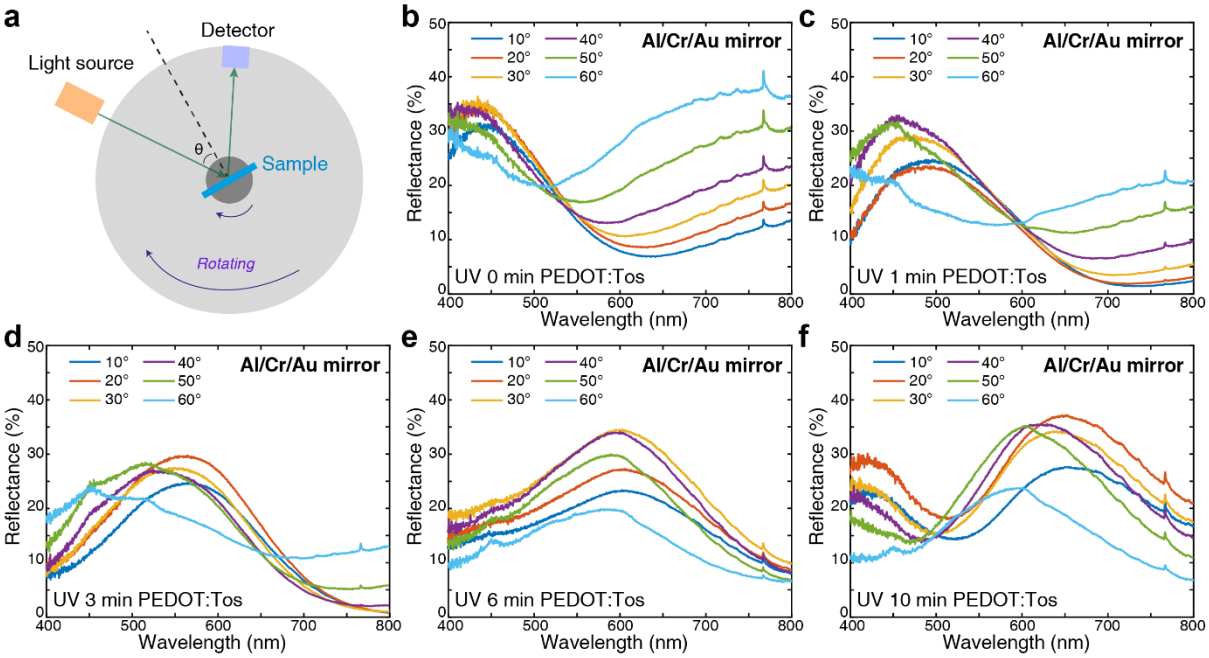

Figure S11 | Incident angle dependence of experimental reflectance spectra. a, The set-up of experimental measurements. A set of concentric wheels were used: the inner wheel was used as a sample holder and the outer one was used to place the detector. **b-f**, The incident angle θ dependence of reflectance spectra for 0, 1, 3, 6, and 10 min UV-treated PEDOT:Tos devices.

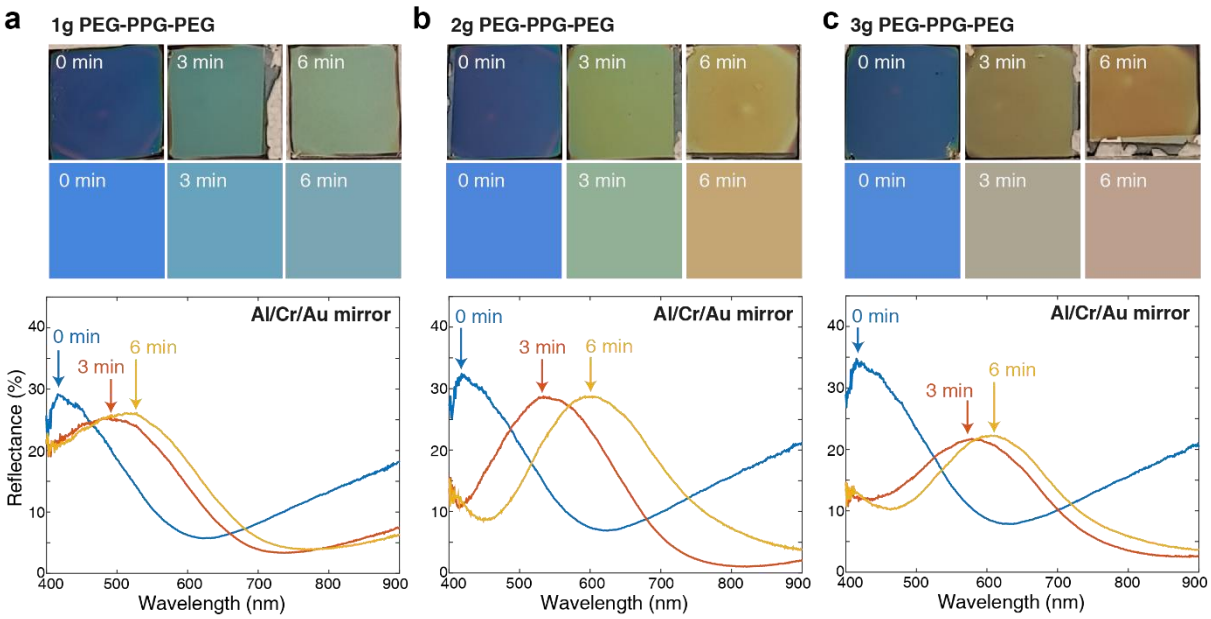

Figure S12 | Influence of precursor recipes on the reflective colors. The concentration of tri-block-co-polymer, PEG-PPG-PEG, in the oxidant solution is tuned with different weight. 1g, 2g, and 3g PEG-PPG-PEG, together with 2g of CB-54 and 5g of ethanol were used. a, b, and c show sample photos (1st row), CIE generated colors (2nd row), and corresponding reflectance spectra (3rd row). All samples were based on 7 nm Au/3 nm Cr/100 nm Al bottom mirror. It is clear that by optimizing the concentration of PEG-PPG-PEG, the UV patterning effect can be tuned including changes in both reflectance peak wavelengths and widths.

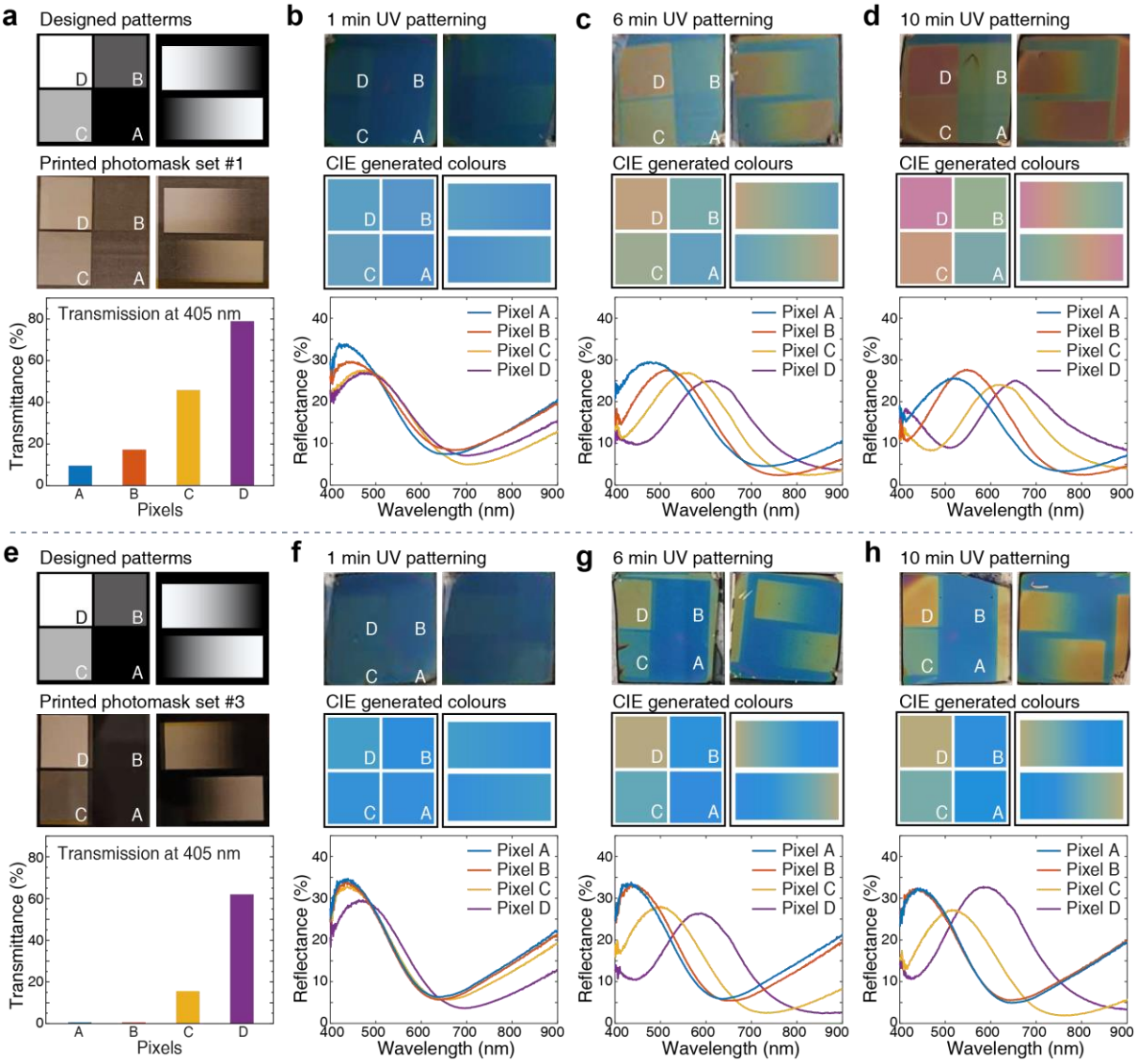

Figure S13| Greyscale photomasks and the corresponding UV-patterned PEDOT devices. a, Designed greyscale photomask patterns with pixels and gradient bars (1st row) and its printed version #1 (2nd row). The 3rd row is the transmittance curves for four pixels in the UV-vis. **b-d**, Sample images, CIE generated colors, and corresponding reflectance spectra for 1, 6, and 10 min UV patterned samples. **e-h**, Photomask set #3 and its resulted samples with 1, 6, and 10 min UV patterning. Since photomasks were printed with a normal office printer and it was difficult to achieve all the greyscale colors within a single printing step. We therefore printed identical patterns on the same photomasks and attempted to overlap them in order to make pixel C and D darker. We denote the 1-time printed, 2-time printed, and 3-time printed photomasks as set #1, #2, and #3 indicated in **Figure 3b**, **Figure S13a**, and **S13e**.

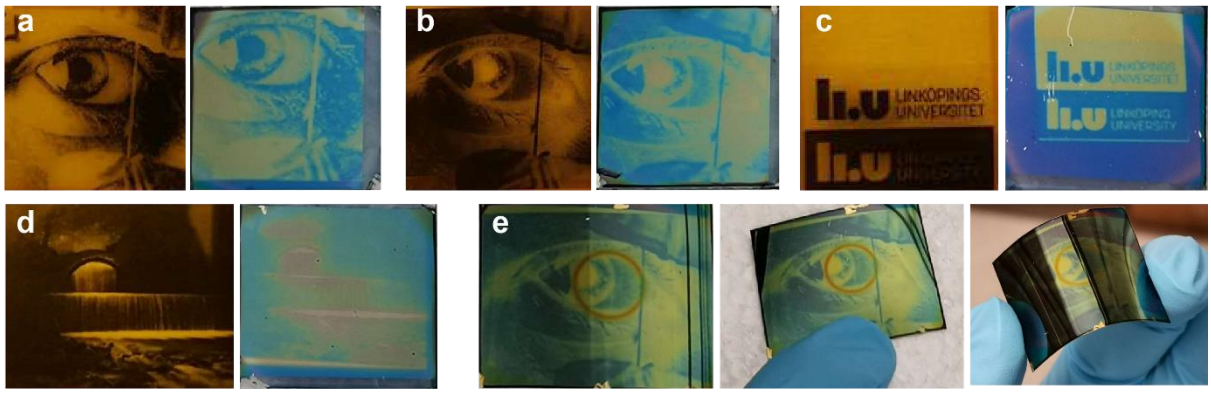

Figure S14 | UV-patterned PEDOT devices using greyscale photomasks. a-d, UV patterned PEDOT devices made on glass substrates (left: greyscale photomasks and right: devices). **e**, UV patterned PEDOT devices made on PET substrates (left: device image, middle: device in an original sate, and right: device in a bent state). The red ring is an artifact related to spin-coating of the oxidant on the flexible PET substrate.

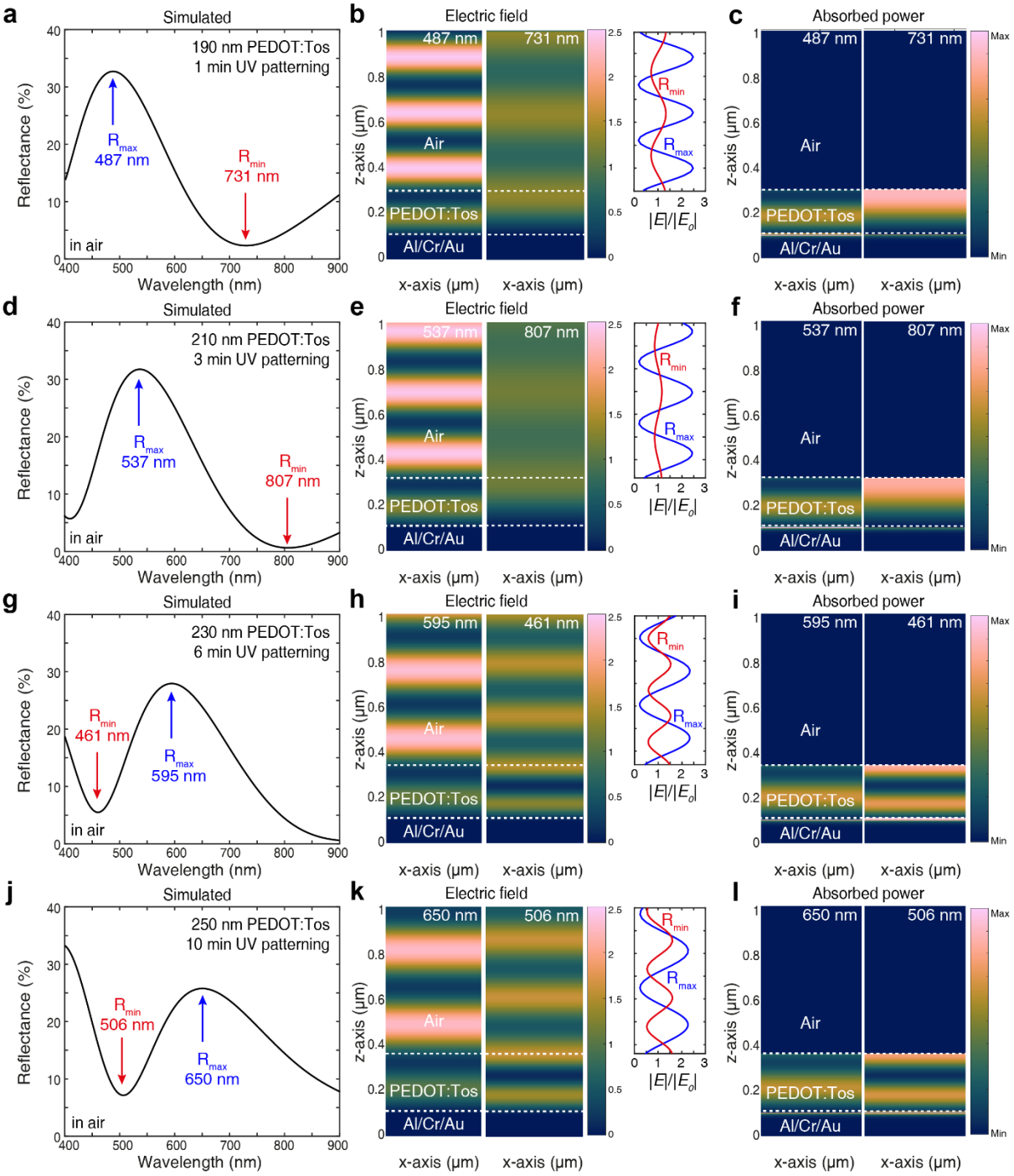

Figure S15 | Electric field and absorbed power distribution of UV-treated PEDOT devices. a, d, g, and **j**, Reflectance spectra of 1 min UV patterned (190 nm), 3 min UV patterned (210 nm), 6 min UV patterned (230 nm), and 10 min UV patterned (250 nm) PEDOT devices. **b**, **e**, **h**, and **k**, Electric field distribution at the reflectance maximum (left column), reflectance minimum (middle column), and the relative electric field strength along *z* axis above the PEDOT surfaces (right column). **c**, **f**, **i**, and **l**, Absorbed power distribution at the reflectance maximum (left column) and reflectance minimum (right column). Wavelengths for reflectance maximum and minimum of each device are indicated in the reflectance spectra.

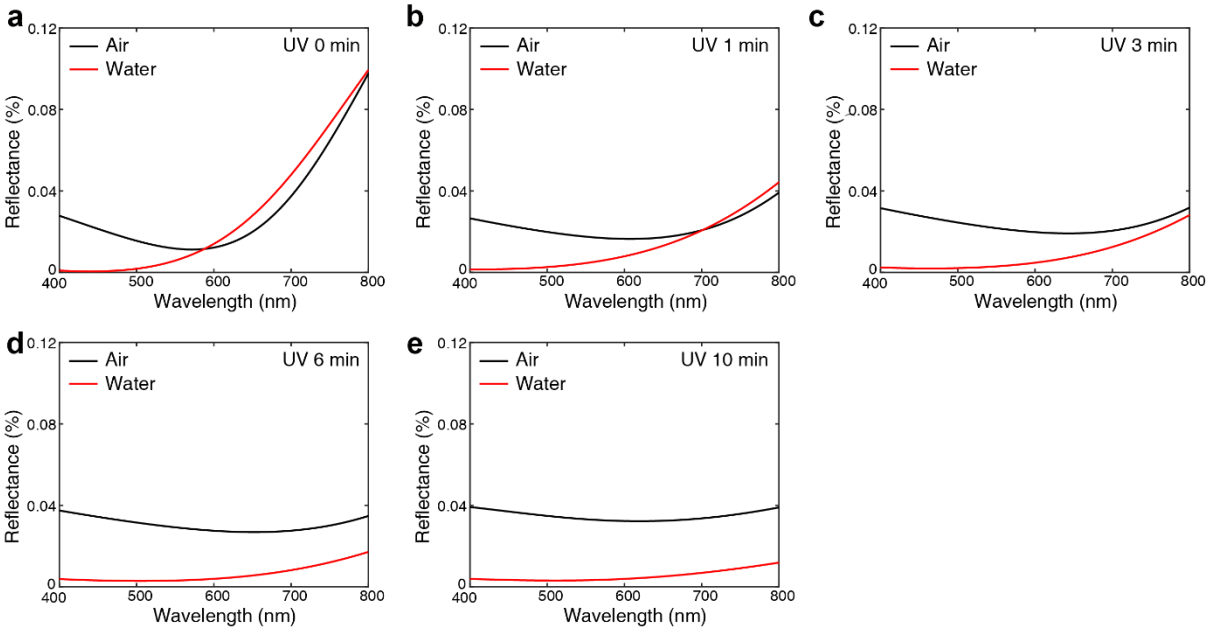

Figure S16 | Simulated reflectance at the interface between air or water and PEDOT for different UV treatments. a-e, Reflectance at the air/PEDOT (black) and water/PEDOT (red) interfaces with UV exposure times of: **a**, 0 min, **b**, 1 min, **c**, 3 min, **d**, 6 min, and **e**, 10 min.

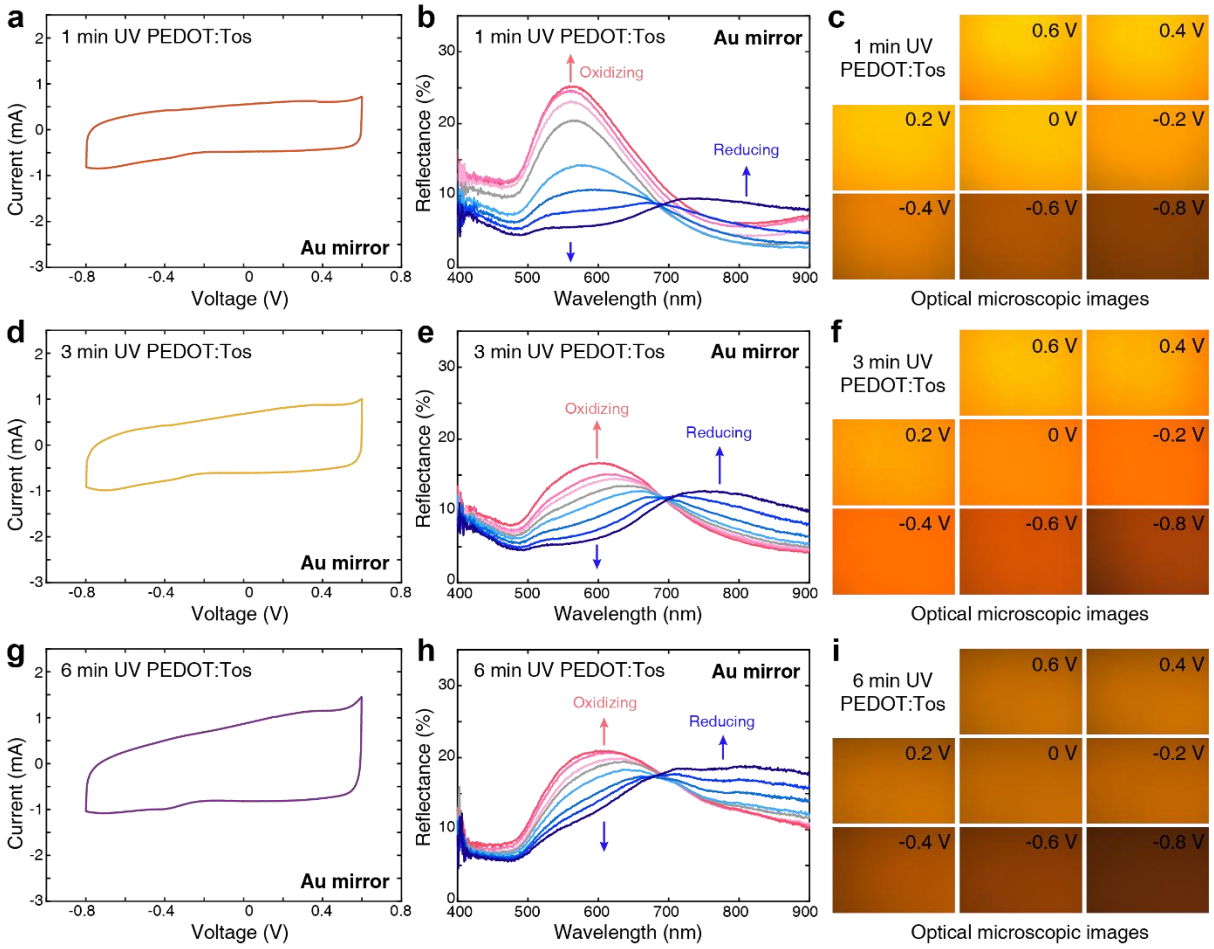

Figure S17 | Electrochemical responses of UV-treated PEDOT displays. a, d, and **g,** Cyclic voltammetry of UV patterned PEDOT films on Au mirrors (**a,** 1 min, **d,** 3 min, and **g,** 6 min). The scan rate was 100 mV/s. **b, e,** and **h,** *In-situ* electrochemical reflectance spectra (**b,** 1 min, **e,** 3 min, and **h,** 6 min). **c, f,** and **i,** Optical microscope images of samples at different electrochemical bias (**c,** 1 min, **f,** 3 min, and **i,** 6 min). The intensity of the line colors represents the absolute values of the electrochemical bias (dark red to light red: 0.6 V, 0.4 V, 0.2 V, and dark blue to light blue: -0.8 V, -0.6 V, -0.4 V, -0.2 V). The grey color curve is for zero electrochemical bias.

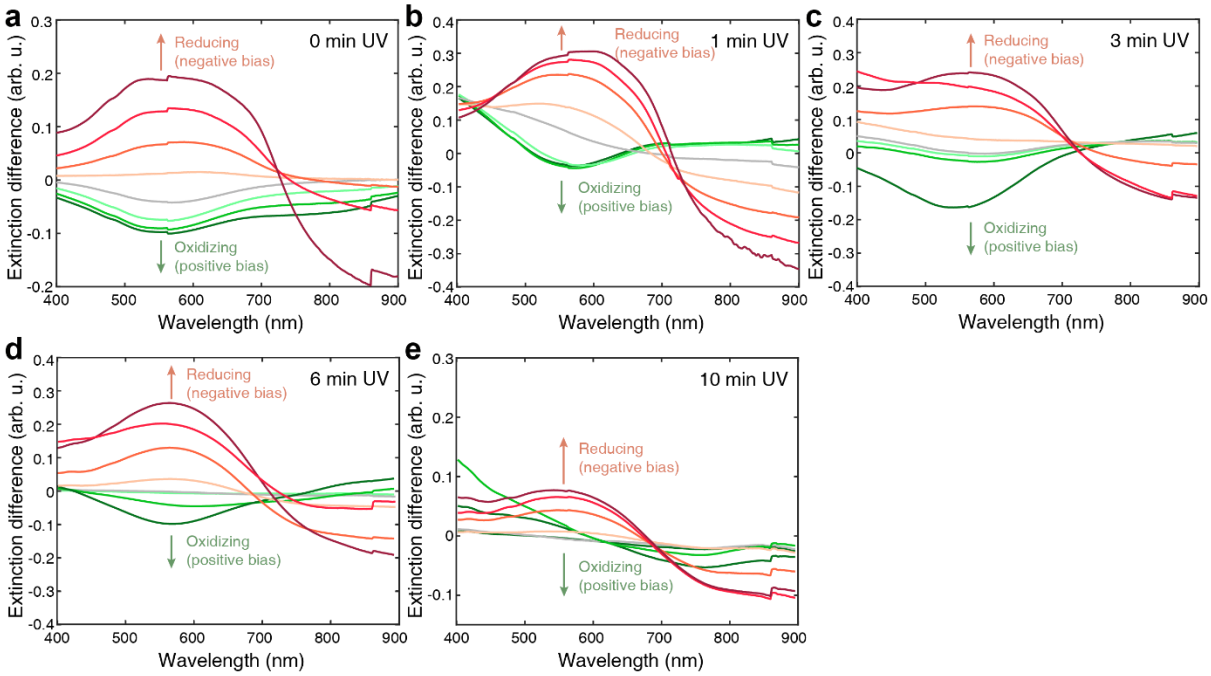

Figure S18 | *In-situ* electrochemical extinction difference spectra of UV-treated PEDOT:Tos films. a, 0 min, **b,** 1 min, **c,** 3 min, **d,** 6 min, and **e,** 10 min UV-treated PEDOT:Tos films. The spectra uses the pristine state PEDOT:Tos without electrochemical bias in the electrolyte as the reference, and measuring the net extinction changes at different electrochemical bias. The sum of the optical extinction and transmission is 1. Green curves (dark to light: 0.6 V, 0.4 V, and 0.2 V) indicate positive electrochemical bias (oxidizing the polymer) and red curves (dark to light: -0.8 V, -0.6 V, -0.4 V, and -0.2V) indicate negative electrochemical bias (reducing the polymer). All the films were deposited on ITO-coated glass substrates.

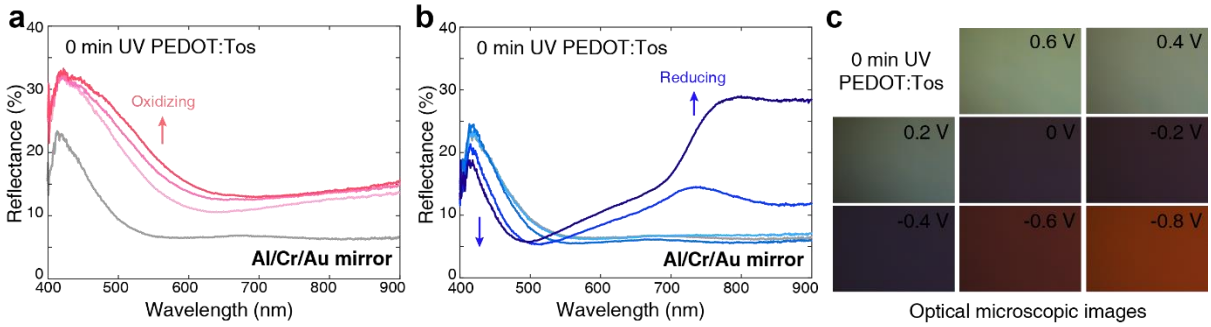

Figure S19 | Electrochemical responses of UV-treated PEDOT displays on Al/Cr/Au mirror. a and **b,** *in-situ* electrochemical reflectance spectra (**a,** oxidation, **b,** reduction). **c,** Optical microscope images of samples at different electrochemical bias. The intensity of the line colors represents the absolute values of the electrochemical bias (dark red to light red: 0.6 V, 0.4 V, 0.2 V, and dark blue to light blue: -0.8 V, -0.6 V, -0.4 V, -0.2 V). Grey color curve is for zero electrochemical bias. However, the Al/Cr/Au mirror was not stable in the electrochemical environment and started to fall off from the substrate after several cycles.

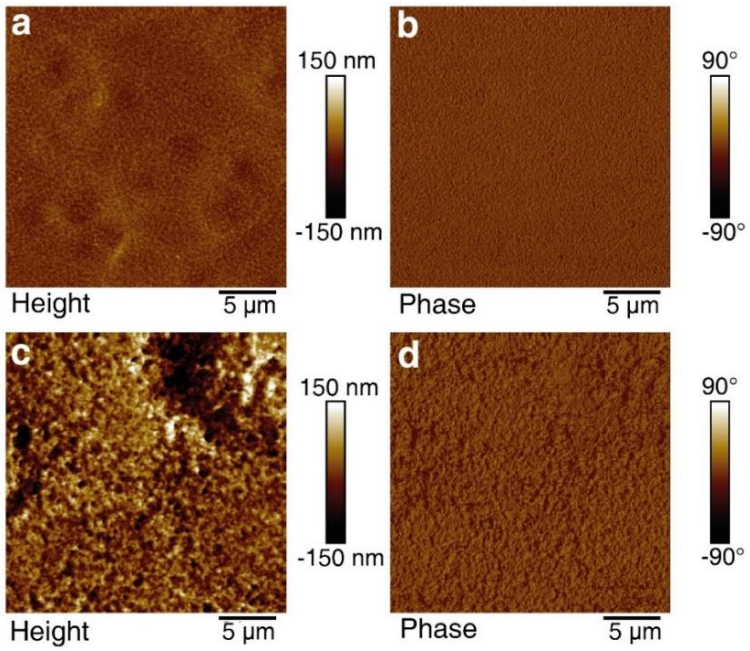

Figure S20 | AFM images of PEDOT:Tos thin films. a and **b**, height and phase images of PEDOT thin films prepared by oxidant without UV exposure. The surface roughness is about 12.5 nm. **c** and **d**, height and phase images of PEDOT prepared with oxidant exposed to UV light for 10 min. The surface roughness is about 46.9 nm.

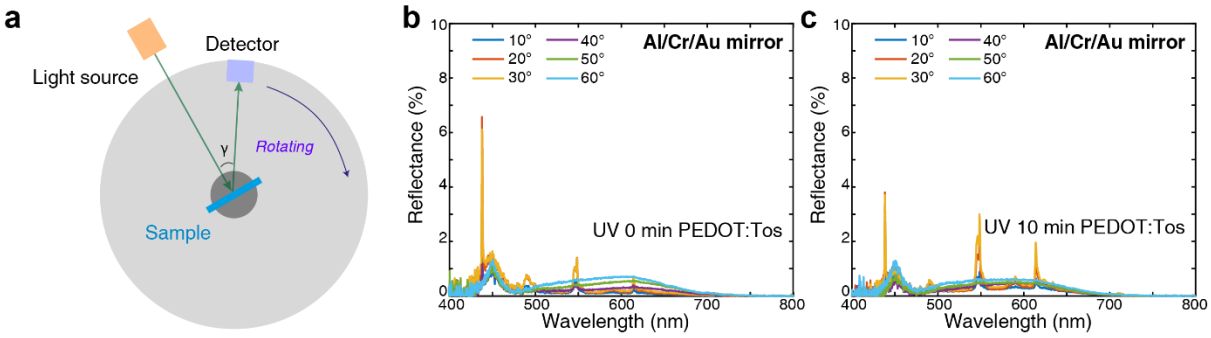

Figure S21 | Experimental scattering reflectance spectra of UV-treated PEDOT:Tos devices. a, The set-up of experimental measurements for normal incidence. **b-c**, Reflectance spectra for 0 min (**b**) and 10 min (**c**) UV-treated PEDOT devices. The scattered light was collected at 10° to 60°. The reflectance mostly stayed below 1 % in the visible (the sharp peaks are attributed to artefacts from measurements).

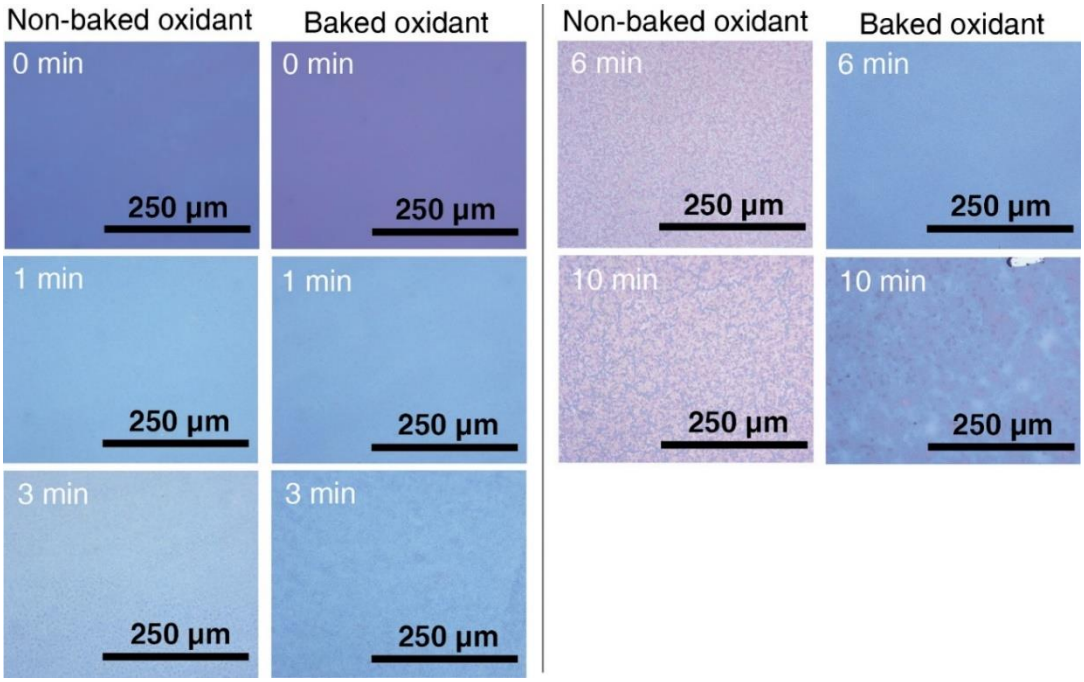

Figure S22 | Optical microscope images of UV-treated PEDOT:Tos films on glass. The UV exposure time was 0, 1, 3, 6, and 10 min. The images were captured in transmission mode. For the non-baked oxidant samples, particle-like features started to emerge after 3 min UV exposure while for baked oxidant sample these features were largely suppressed.

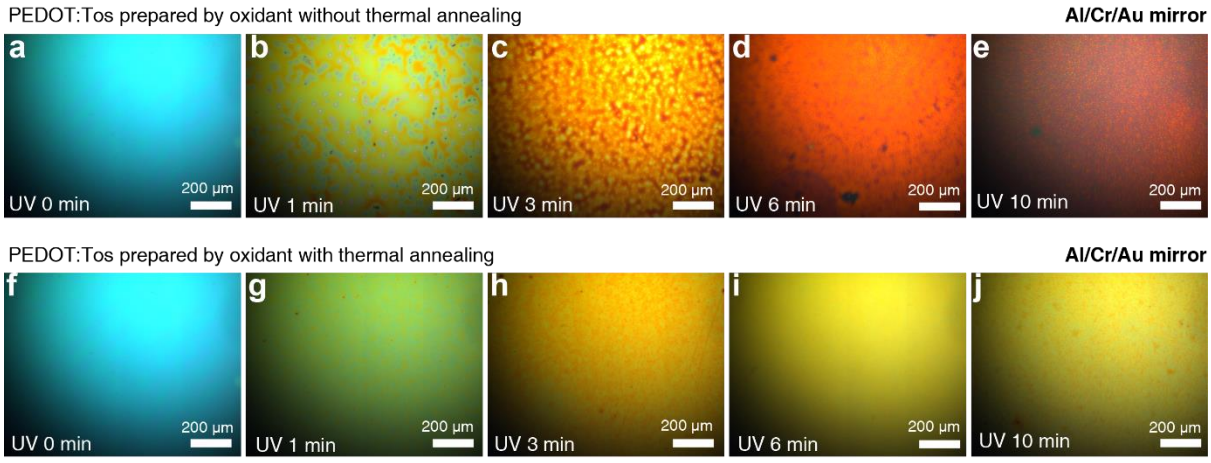

Figure S23 | Optical microscope images of UV-treated PEDOT:Tos devices. a-e, UV patterned PEDOT devices made with non-annealed oxidant. **f-j,** UV patterned PEDOT device made with annealed oxidant. The devices used 7 nm Au/3 nm Cr/100 nm Al mirror. UV exposure times were: 0 min (**a, f**), 1 min (**b, g**), 3 min (**c, h**), 6 min (**d, i**), and 10 min (**e, j**). The microscope images were taken in reflection mode.

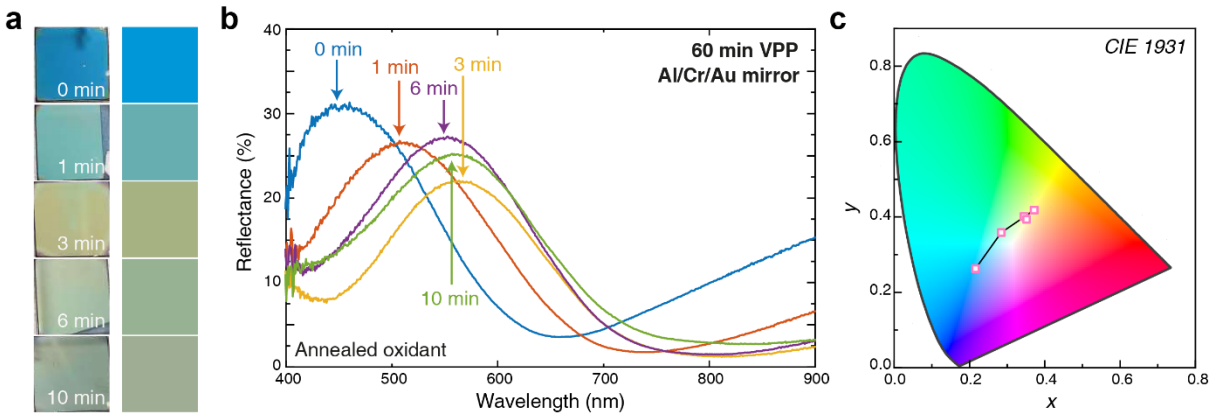

Figure S24 | UV-treated PEDOT:Tos devices based on thermally annealed oxidant. a, Device images (left) and pseudocolors from CIE coordinates based on experimental reflectance curves. **b,** Experimental reflectance curves of the devices on 7 nm Au/3 nm Cr/100 nm Au mirror. **c,** The distribution of corresponding CIE coordinates in *CIE 1931* chromaticity diagram. The UV exposure times were: 0 min, 1 min, 3 min, 6 min, and 10 min.

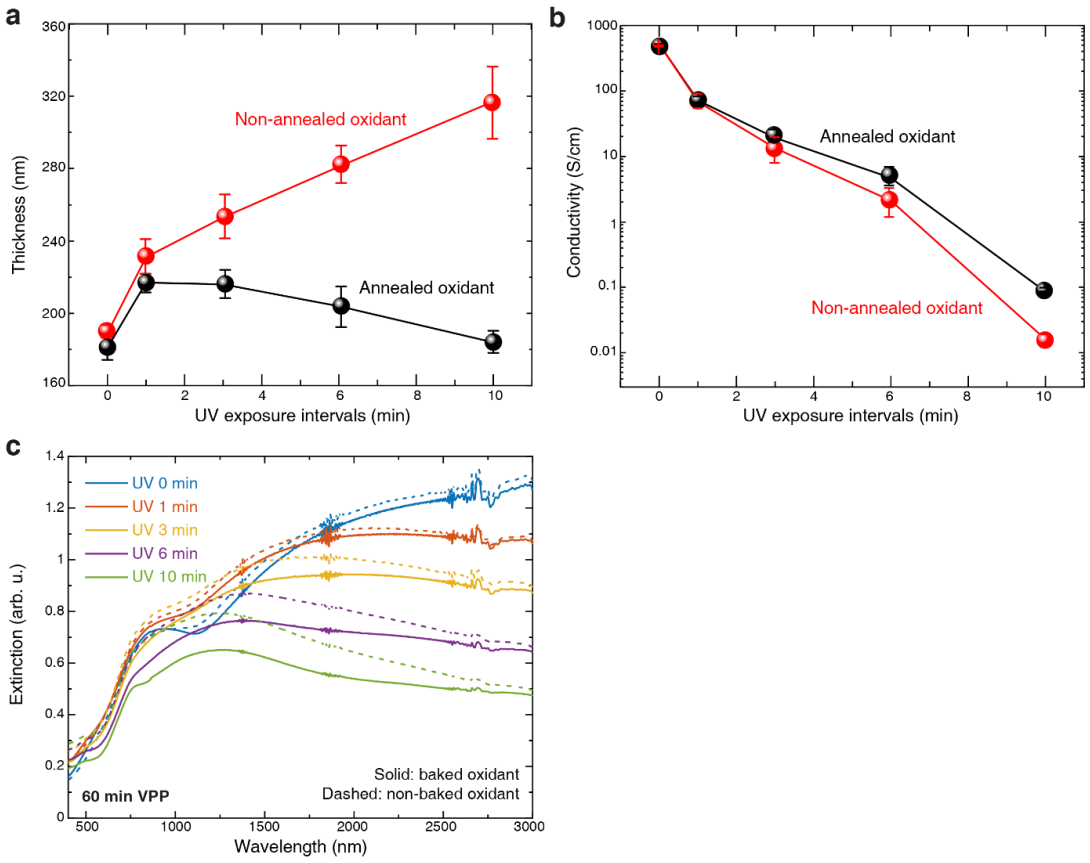

Figure S25 | Properties of UV-treated PEDOT thin films with and without oxidant thermal annealing. a, Film thickness and **b**, electrical conductivity variations. The red curves are films made with non-annealed oxidant and the black curves are those prepared with annealed oxidant. **c**, Optical extinction spectra for UV-treated PEDOT made by oxidants with (solid) and without thermal annealing (dashed).

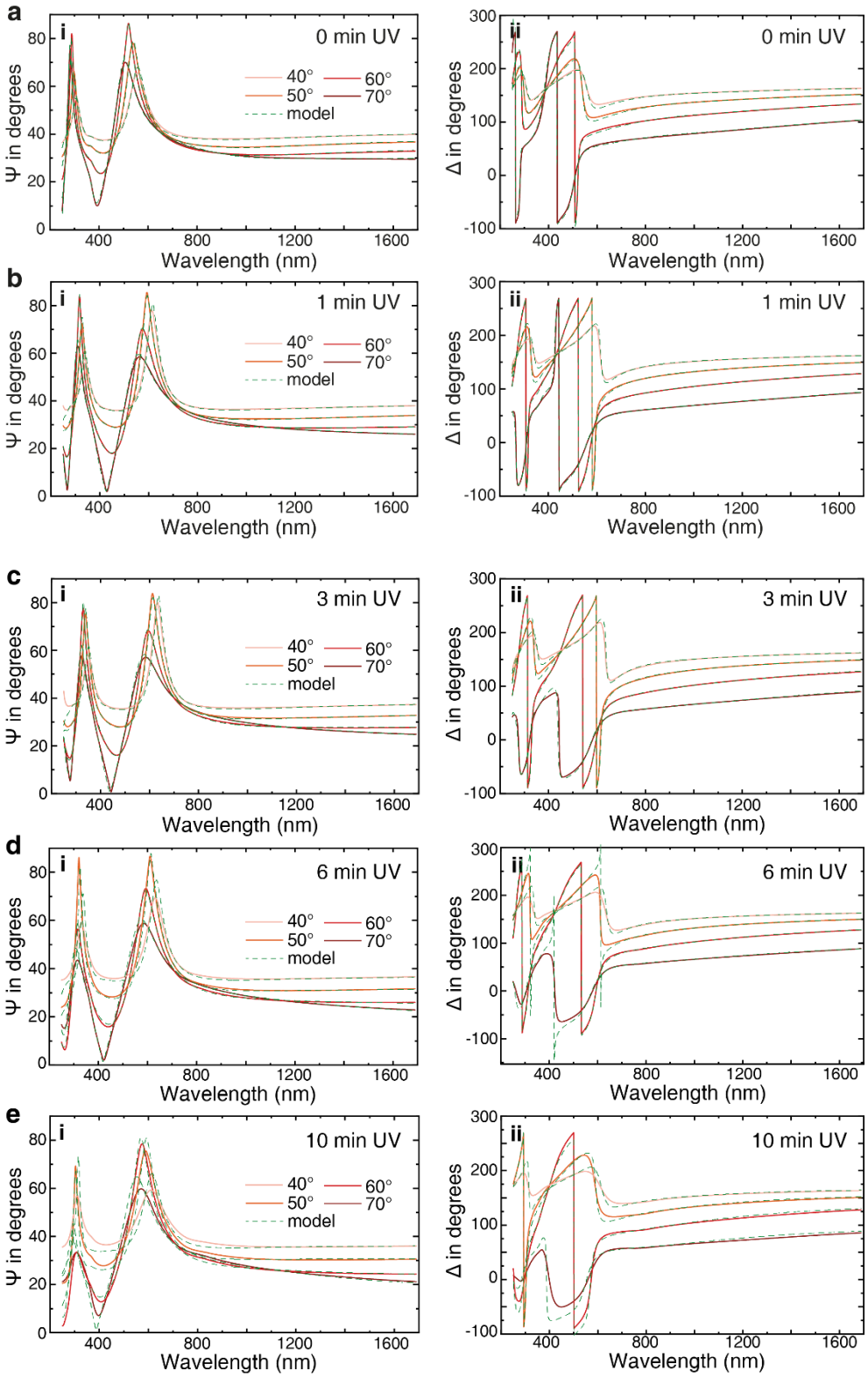

Figure S26 | Spectroscopic ellipsometry spectra for PEDOT:Tos films using UV-exposed oxidants with post-baking. Five UV exposure times were used: 0 min (**a**), 1 min (**b**), 3 min (**c**), 6 min (**d**), and 10 min (**e**). For each measurement, four incident angles were used: 40°, 50°, 60°, and 70°. The experimental measured data (**i** for ψ and **ii** for Δ) and model fits are plotted in solid and dashed curves. All the samples were deposited on silicon wafers coated with 100 nm Au films.

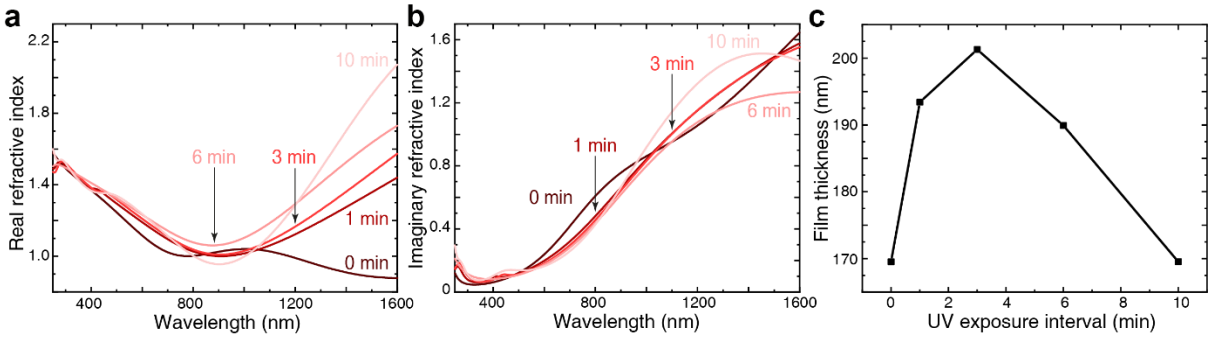

Figure S27 | Properties of UV-treated PEDOT made with annealed oxidants. a, In-plane real refractive index. **b**, In-plane imaginary refractive index. **c**, Thickness of the UV-patterned PEDOT determined by ellipsometry. UV exposure times of 0 min, 1 min, 3 min, 6 min, and 10 min were used.

References

1 Edberg, J. *et al.* Patterning and conductivity modulation of conductive polymers by UV light exposure. *Advanced Functional Materials* **26**, 6950-6960 (2016).

2 Brooke, R. *et al.* Controlling the electrochromic properties of conductive polymers using UV-light. *Journal of Materials Chemistry C* **6**, 4663-4670 (2018).

3 Fabretto, M., Zuber, K., Hall, C., Murphy, P. & Griesser, H. J. The role of water in the synthesis and performance of vapour phase polymerised PEDOT electrochromic devices. *Journal of Materials Chemistry* **19**, 7871-7878 (2009).

4 Mueller, M. *et al.* Vacuum vapour phase polymerization of high conductivity PEDOT: Role of PEG-PPG-PEG, the origin of water, and choice of oxidant. *Polymer* **53**, 2146-2151 (2012).

5 Chen, S. *et al.* On the anomalous optical conductivity dispersion of electrically conducting polymers: ultra-wide spectral range ellipsometry combined with a Drude–Lorentz model. *Journal of Materials Chemistry C* **7**, 4350-4362 (2019).

6 Chen, S. *et al.* Unraveling vertical inhomogeneity in vapour phase polymerized PEDOT: Tos films. *Journal of Materials Chemistry A* **8**, 18726-18734 (2020).